Available online at www.sciencedirect.com
ScienceDirect
Journal of Sound and Vibration 315 (2008) 34–57
JOURNAL OF SOUND AND VIBRATION
www.elsevier.com/locate/jsvi

New online payload identification for flexible robots. Application to adaptive control

Francisco Ramos*, Vicente Feliu

ETSI Industriales, Edificio Politécnico, Universidad de Castilla-La Mancha, Ciudad Real 13071, Spain

Received 23 October 2007; received in revised form 31 January 2008; accepted 1 February 2008
Handling Editor: C. Morfey
Available online 9 April 2008

Abstract

This work presents a new method for online payload identification of single-link flexible robots. Presented technique takes as inputs the measurements of the motor position and the coupling torque at the base of the beam measured by means of a strain gauge. With a simple and effective management of these data, we are able to accurately estimate the tip mass. Simulation results demonstrate the goodness of this technique. Subsequently, a proportional-derivative (PD) adaptive control scheme which uses the information from the identification method has been developed and a set of experiments have been carried out in a real platform.

1. Introduction

Flexible robots became one of the most challenging fields in control engineering since they were conceived and they have attracted a lot of interest, as shown in recent surveys on modeling and control of flexible manipulators [1,2]. Their benefits when compared with the traditional industrial robots are unquestionable: less weight which means less amount of material, less energy requirement to be actuated, less damage in case of impact; while more speed, more ratio payload/weight. However, their inherent vibrational nature convert them in elements difficult to position accurately, needing then complex control schemes to be driven in rest-to-rest maneuvers, not to talk about trajectory tracking. Even more, these arms are intrinsically non-minimum phase systems and, with the most intuitive sensorial configurations, which directly measure the tip position (e.g. accelerometers), non-collocated systems also.

However, some engineering fields cannot afford the use of heavier robots. The best example is the aerospace industry. Even if these kinds of manipulators have multiple applications, (e.g. mobile vehicles, disk drive heads or robotic surgery) none of them has impelled the development of the control schemes for flexible robots as the aerospace industry. The Space Station Remote Manipulator System (SSRMS) is the best example of the achievements in this area [3].

*Corresponding author.
E-mail addresses: Francisco.Ramos@uclm.es (F. Ramos), Vicente.Feliu@uclm.es (V. Feliu).

0022-460X/$ - see front matter © 2008 Elsevier Ltd. All rights reserved.
doi:10.1016/j.jsv.2008.02.003

Nomenclature

$\mathbf{A}$	stiffness matrix of the beam model
c	beam stiffness
$D(s)$	denominator of the mass estimator
$\tilde{D}(s)$	denominator of the mass estimator after applying the low-pass filter
E	Young's modulus
$F(s)$	low-pass filter
F_t	external force applied to the payload
$g_{ij}(s)$	transfer function of the beam model
$g^n{}_j(s)$	normalized transfer function of the beam model
$G(s)$	matrix of transfer functions of the beam model
I	cross-section inertia of the beam
J_m	motor inertia
K	DC motor constant
K_p	constant of the proportional part of the PD motor controller
K_v	constant of the derivative part of the PD motor controller
l	beam length
m	tip mass
m_b	beam mass
$\mathbf{M}$	mass matrix of the beam model
$M(s)$	motor loop dynamics
n	number of masses in the lumped masses model for the flexible link
n_r	reduction relation of the gear
$N(s)$	numerator of the mass estimator
$\tilde{N}(s)$	numerator of the mass estimator after applying the low-pass filter
r	radius of the link of the flexible robot
s	Laplace domain variable
T	sampling time of the data acquisition system
V	control signal for the DC motor
z	discrete domain variable
α	motor dynamics parameter
Γ_c	coupling torque between motor and beam
Γ_m	torque generated by the actuator
θ_i	angle to mass at point i
θ_m	motor angle
θ_t	tip angle
$\mathbf{\Theta}$	vector of concentrated masses angles
λ	relation between beam mass and tip mass
v	viscous friction coefficient
ω_f	cut-off frequency for the low-pass filter

Many of the developed controllers depend strongly on the exact modeling of the mechanical system. Any change in the plant parameters reduces the controller performance, making the system lose the desired specifications. Actually, the payload, which is one of the most determinant parameters in robot dynamics, may change very often in a robotic system under normal operation, either for changing the tip tool being used, or for grasping an object with non-negligible weight. Therefore, the controller needs to be as robust as possible with respect to this common variation.

A number of different strategies have been applied to overcome this drawback, which can be grouped into three big categories of control theory. Namely, *intelligent control*, based on techniques with the ability to learn, such as neural networks or genetic algorithms, which are usually very demanding computationally due to its nonlinear intrinsic nature; *robust control*, e.g. H_∞ control, which provides schemes that perform correctly under a certain range of parameter uncertainties; and a major effort has been devoted to the development of *adaptive control* schemes.

Adaptive control is a nonlinear control strategy that varies the values of the controller parameters, depending on some criteria based upon the data collected from the previous movements, to achieve an optimal performance even when the changes in the plant are significant. A classification of the different adaptive schemes is detailed in Ref. [4], where four types are described: *gain scheduling*, which adjusts controller parameters on the basis of the operating conditions which change during the process; *model-reference adaptive systems* (MRAS) which compare the actual system output and the model output and modify the controller so that the error between them is small; *self-tuning regulators* (STR), which update the system parameters from the estimation process and obtain the controller constants from the solution of a design problem using the estimated parameters; and *dual control schemes*, where nonlinear stochastic control theory is used for achieving the abstract problem formulation.

Several of these adaptive schemes have been proposed in literature for controlling flexible robots, usually based in a two-stage process in which the adaptation of the controller is preceded by a system identification

stage [5,6]. Some of these controllers need to recalculate the whole model, e.g. the MRAS proposed in Ref. [7] for a single-link flexible arm, or the passivity-based control approach of the MRAS presented in Refs. [8,9] for the multilink case. Ref. [8] presents a numerical example based on a model of the Shuttle Remote Manipulator System (SRMS), where all the payload mass properties are identified, while in Ref. [9] the previous adaptive scheme is extended with an identification stage that also determines the arm mass properties and presents experimental results on a planar 3-link flexible manipulator. However, this solution may become considerably inefficient, as most of the parameters do not change its value for long periods of time, and other authors have proposed different STRs, focusing this identification stage in a specific, representative parameter of the system, which serves to redesign the set of controller constants to keep the desired system specifications. In Ref. [10], the identification process focuses in identifying the payload, which as aforementioned, is the most variable parameter in the usual operation of a robotic arm. The proposed estimator is based on the measurements from an accelerometer placed at the payload and the control signal. That work has, however, some inaccuracies because it includes the motor dynamics in the estimation process, which involves the parameters of the motor, rotor inertia and viscous friction, and the Coulomb friction. While the rotor inertia remains unchanged, the viscous friction is strongly dependant with temperature, and varies even along a single maneuver. On the other hand, the Coulomb friction inserts a strong nonlinearity in the identification process, which is difficult to pre-compensate accurately and may cause an inexact estimation. A different approach is taken by Trapero et al. [11] for the identification stage. They propose a frequency estimator based on an algebraic method that has the drawback that it can only be applied to sinusoid-like signals, and hence, it can only be applied to the identification of the system frequencies while the robot actuator is stopped and the link is vibrating steadily.

In the present work, a different payload estimator is proposed. This estimator solves abovementioned drawbacks, needs small computational effort and gives good accuracy, while can be applied during the robot maneuver. Similarly to the algebraic estimator proposed in Ref. [11], the identification process is carried out using a continuous-time frame instead of a discrete-time model for a number of reasons (see Refs. [12,13]): it preserves the a priori knowledge of the system and gives a better understanding of the physical behavior of the system and the estimation is less sensitive to sampling frequencies and initial conditions.

The sensorial system used is different from the one used in Ref. [10], and consists of a couple of strain gauges, which measure the coupling torque at the motor end of the beam due to inertial forces, and an incremental encoder, which senses the motor angle. The use of these two sensors prevents motor dynamics from affecting the estimator calculations and, hence, makes the identification process more robust.

The rest of the article is organized as follows. Section 2 describes the general expression of the estimator for a lumped masses model with n masses system model, which is commonly used for describing a flexible robot, while Section 3 particularizes the previous estimation for the single mass and two masses models, from where some interesting conclusions for the sake of simplicity can be inferred. Next, Section 4 simulates the behavior of an estimator designed for a specific model and also shows the performance of a reduced order estimator when dealing with higher order models for the beam. The experimental platform is detailed in Section 5, where a set of experimental results supporting the goodness of the method are also displayed and applied to an adaptive proportional derivative (PD) controller based on the identification process. Finally, some conclusions are stated in Section 6.

2. Estimation algorithm

In the first place, an estimator for the tip mass, which is totally independent of the robot model, is developed. Subsequently, a general lumped masses model for a flexible beam is presented and finally the estimator is specifically obtained for that model.

2.1. General payload estimator expression

We will assume that our flexible beam is a multiinput multioutput (MIMO) system that can be outlined with the black box scheme shown in Fig. 1, where our plant will be determined by a matrix of transfer functions

according to the following expression:

$$\begin{bmatrix} \theta_t \\ \Gamma_c \end{bmatrix} = \underbrace{\begin{bmatrix} g_{11}(s) & g_{12}(s) \\ g_{21}(s) & g_{22}(s) \end{bmatrix}}_{G(s)} \begin{bmatrix} \theta_m \\ F_t \end{bmatrix} \tag{1}$$

with the additional relation

$$F_t(s) = -mls^2\theta_t(s) \tag{2}$$

corresponding to the inertial force existent at the tip of the arm as a consequence of accelerating the payload. This relation reduces the complexity of system (1) to a singleinput multioutput system whose state can be determined by simply using θ_m. Notice that parameters of $G(s)$ are independent of the tip payload. They depend on the link geometry, link elasticity and masses located on the link (with the exception of the tip).

The estimation algorithm will prove to be motor independent, and, therefore, motor dynamics have not been included in the model.

Let us suppose that θ_m and Γ_c are given by our sensorial system. Taking this hypothesis as a premise, and operating in Eq. (1), we can find expressions for θ_t and F_t dependant on the measured variables. Concretely,

$$\begin{bmatrix} \theta_t(s) \\ F_t(s) \end{bmatrix} = \frac{1}{g_{22}(s)} \begin{bmatrix} g_{11}(s)g_{22}(s) - g_{12}(s)g_{21}(s) & g_{12}(s) \\ -g_{21}(s) & 1 \end{bmatrix} \begin{bmatrix} \theta_m(s) \\ \Gamma_c(s) \end{bmatrix} \tag{3}$$

On the other hand, we can clean up the additional relation (2) yielding a general estimator for the tip mass

$$m = -\frac{1}{l}\frac{F_t(s)}{s^2\theta_t(s)} \tag{4}$$

Joining the expressions given by Eq. (3) with the estimator obtained in Eq. (4), we can derive a general expression in terms of the measured variables. That is

$$m = \frac{N(s)}{D(s)} = \frac{1}{ls^2}\frac{g_{21}(s)\theta_m(s) - \Gamma_c(s)}{(g_{11}(s)g_{22}(s) - g_{12}(s)g_{21}(s))\theta_m(s) + g_{12}(s)\Gamma_c(s)} \tag{5}$$

This formulation is independent of the particular form of g_{ij} transfer functions, i.e. it is valid for any model that can be expressed in the form presented in Eq. (1).

2.2. General lumped masses model

Now we need to provide a model for the estimator deduced in the previous section. A general lumped masses model is proposed to obtain a particular expression for Eq. (5). However, this expression is still general for an arbitrary number of masses, depending on the accuracy we need in our model to describe correctly the physical setup. The beam model used along the paper, which is outlined in Fig. 2, has been presented in previous literature (e.g. in Ref. [14]), but it will be briefly introduced for completion sake. A more detailed description can be found in the reference.

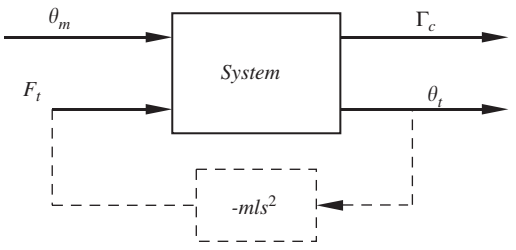

Fig. 1. Black box MIMO for the flexible beam.

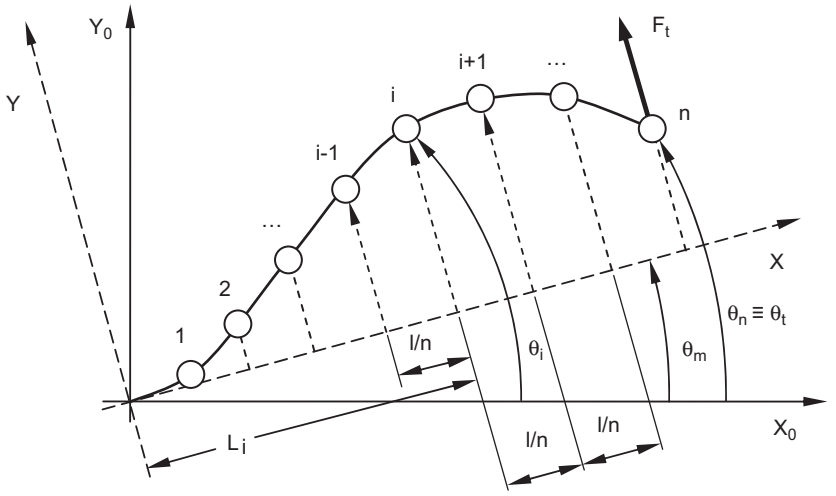

Fig. 2. Scheme of the general lumped masses model.

Prior to presenting the model, a number of vectors and matrices are presented in following equations for the sake of simplicity:

$$\mathbf{U}_i = \begin{bmatrix} 1 \\ 1 \\ \vdots \\ 1 \end{bmatrix}, \quad \hat{\mathbf{U}}_i = \begin{bmatrix} 0 \\ \vdots \\ 0 \\ 1 \end{bmatrix}, \quad \overline{\mathbf{U}}_i = \begin{bmatrix} 1 \\ \vdots \\ 1 \\ 0 \end{bmatrix} \quad \Rightarrow \quad \mathbf{U}_i = \hat{\mathbf{U}}_i + \overline{\mathbf{U}}_i; \quad \mathbf{U}_i,\ \hat{\mathbf{U}}_i,\ \overline{\mathbf{U}}_i \in \Re^{i\times 1} \tag{6}$$

$$\mathbf{I}_i = \begin{bmatrix} 1 & & 0 \\ & \ddots & \\ 0 & & 1 \end{bmatrix} \quad \hat{\mathbf{I}}_i = \begin{bmatrix} 1 & & 0 \\ & \ddots & \\ 0 & & 1 \\ 0 & \cdots & 0 \end{bmatrix} \quad \Rightarrow \quad \mathbf{I}_i = [\hat{\mathbf{I}}_i | \hat{\mathbf{U}}_i]; \quad \mathbf{I}_i \in \Re^{i\times i}, \quad \hat{\mathbf{I}}_i \in \Re^{i\times i-1} \tag{7}$$

$$\mathbf{\Theta}_i = \begin{bmatrix} \theta_1 \\ \theta_2 \\ \vdots \\ \theta_i \end{bmatrix}, \quad \mathbf{\Lambda}_i = \frac{1}{n^2}[\,1 \quad 4 \quad \cdots \quad (i-1)^2 \quad i^2\,] \quad \Rightarrow \quad \mathbf{\Theta}_i \in \Re^{i\times 1}, \quad \mathbf{\Lambda}_i \in \Re^{1\times i} \tag{8}$$

Along the paper, the subindex of these matrices makes reference to their dimensions and θ_n will be denoted as θ_t, as it represents the tip angle.

The presented model assumes that the mass is concentrated in a finite number of points, n, and that the links between these points are massless. It also assumes that the rotary inertia of each mass is negligible and, hence, the number of vibration modes will be equal to the number of masses considered. In addition, we assume that the payload produces no torque at the tip. All the angles are measured from a fixed reference frame X_0-Y_0. With these hypothesis two matrix equations can be obtained that relate the robot dynamics with the inputs of the system, namely, the motor angle and the tip force. The equations are

$$\mathbf{M}_n\ddot{\mathbf{\Theta}}_n = \frac{EI}{l^3}\mathbf{A}_n[\mathbf{U}_n\theta_m - \mathbf{\Theta}_n] + \frac{1}{l}\hat{\mathbf{U}}_n F_t \tag{9}$$

$$\Gamma_c = l^2\mathbf{\Lambda}_n\mathbf{M}_n\ddot{\mathbf{\Theta}}_n - lF_t \tag{10}$$

Assuming that the total beam mass is a portion of the payload, $m_b = \lambda m$, and that it is equally divided in the $n-1$ intermediate points which are equidistant with distance l/n, the mass matrix of the beam can be expressed as

$$\mathbf{M}_n = \frac{\lambda m}{n-1}\begin{bmatrix} 1 & 0 & \cdots & 0 \\ 0 & \ddots & \ddots & \vdots \\ \vdots & \ddots & 1 & 0 \\ 0 & \cdots & 0 & 0 \end{bmatrix} \tag{11}$$

and the reduced mass matrix is

$$\mathbf{M}_{n-1} = \frac{\lambda m}{n-1}\begin{bmatrix} 1 & & 0 \\ & \ddots & \\ 0 & & 1 \end{bmatrix} \tag{12}$$

being $\mathbf{M}_n \in \Re_{n\times n}$ and $\mathbf{M}_{n-1} \in \Re_{n-1\times n-1}$. On the other hand, $\mathbf{A}_n$ is a dimensionless matrix, which must be calculated, depending on the geometric properties of the beam (distance between masses, relative mass of each point and distance from each mass to the motor), by applying the continuity conditions for all the point masses, as shown in Ref. [14], for example. Finally, $l^2\mathbf{\Lambda}_n$ is the vector of distances measured from the motor.

2.3. Obtaining the g_{ij} transfer functions

This subsection presents the calculations necessary to derive the expressions of the transfer functions, which define our system. Basically, we will divide the system into two parts. The first one is the last row of Eq. (9), which involves the tip angle and the external force. The second one is the $n-1$ remaining equations, which involve only the intermediate masses in which the beam is divided. We operate these two subsystems to obtain the general equations of the system model presented in (1) and, hence, the g_{ii} transfer functions.

Then, if we extract the last row of Eq. (9), that is

$$0 = \frac{EI}{l^3}\hat{\mathbf{U}}_n^{\mathbf{T}}\mathbf{A}_n[\mathbf{U}_n\theta_m - \mathbf{\Theta}_n] + \frac{1}{l}F_t \tag{13}$$

and then we rearrange the equation making use of the definitions given in Eqs. (6), (7) and (8), we obtain the following expression for the tip angle:

$$\theta_t = \theta_m + \frac{\hat{\mathbf{U}}_n^{\mathbf{T}}\mathbf{A}_n\hat{\mathbf{I}}_n}{\hat{\mathbf{U}}_n^{\mathbf{T}}\mathbf{A}_n\hat{\mathbf{U}}_n}(\mathbf{U}_{n-1}\theta_m - \mathbf{\Theta}_{n-1}) + \frac{1}{\hat{\mathbf{U}}_n^{\mathbf{T}}\mathbf{A}_n\hat{\mathbf{U}}_n}\frac{l^2}{EI}F_t \tag{14}$$

where $\mathbf{U}_n^{\mathbf{T}}$ represents the transpose of $\mathbf{U}_n$.

Taking into consideration only the first $n-1$ equations, expression (9) yields

$$\mathbf{M}_{n-1}\ddot{\mathbf{\Theta}}_{n-1} = \frac{EI}{l^3}\hat{\mathbf{I}}_n^{\mathbf{T}}\mathbf{A}_n[\mathbf{U}_n\theta_m - \mathbf{\Theta}_n] = \frac{EI}{l^3}\hat{\mathbf{I}}_n^{\mathbf{T}}\mathbf{A}_n[\mathbf{U}_n\theta_m - \hat{\mathbf{I}}_n\mathbf{\Theta}_{n-1} - \hat{\mathbf{U}}_n\theta_t] \tag{15}$$

Substituting the value of θ_t given by Eq. (14) into the previous equation, and rearranging terms, we obtain

$$\ddot{\mathbf{\Theta}}_{n-1} = \frac{n-1}{\lambda m}\frac{EI}{l^3}\hat{\mathbf{I}}_n^{\mathbf{T}}\mathbf{A}_n\left(\mathbf{I}_n - \hat{\mathbf{U}}_n\frac{\hat{\mathbf{U}}_n^{\mathbf{T}}\mathbf{A}_n}{\hat{\mathbf{U}}_n^{\mathbf{T}}\mathbf{A}\hat{\mathbf{U}}_n}\right)\hat{\mathbf{I}}_n(\mathbf{U}_n\theta_m - \mathbf{\Theta}_n) - \frac{n-1}{\lambda m}\frac{\hat{\mathbf{I}}_n^{\mathbf{T}}\mathbf{A}_n\hat{\mathbf{U}}_n}{\hat{\mathbf{U}}_n^{\mathbf{T}}\mathbf{A}_n\hat{\mathbf{U}}_n}F_t \tag{16}$$

which can be shortened to

$$\ddot{\mathbf{\Theta}}_{n-1} = \frac{n-1}{\lambda m}\frac{EI}{l^3}\mathbf{A}_{n-1}(\mathbf{U}_n\theta_m - \mathbf{\Theta}_n) - \frac{n-1}{\lambda m}\mathbf{P}_{n-1}F_t \tag{17}$$

where

$$\mathbf{A}_{n-1} = \hat{\mathbf{I}}_n^{\mathrm{T}}\mathbf{A}_n\left(\mathbf{I}_n - \frac{\hat{\mathbf{U}}_n\hat{\mathbf{U}}_n^{\mathrm{T}}\mathbf{A}_n}{\hat{\mathbf{U}}_n^{\mathrm{T}}\mathbf{A}_n\hat{\mathbf{U}}_n}\right)\hat{\mathbf{I}}_n, \quad \mathbf{A}_{n-1} \in \Re_{(n-1)\times(n-1)}, \quad \mathbf{P}_{n-1} = \frac{\hat{\mathbf{I}}_n^{\mathrm{T}}\mathbf{A}_n\hat{\mathbf{U}}_n}{\hat{\mathbf{U}}_n^{\mathrm{T}}\mathbf{A}_n\hat{\mathbf{U}}_n}, \quad \mathbf{P}_{n-1} \in \Re_{(n-1)\times 1} \tag{18}$$

Transforming Eq. (17) into the Laplace domain, we have

$$\hat{\mathbf{\Theta}}_{n-1}(s) = \left(\mathbf{I}_{n-1}\frac{s^2}{\omega^2} + \mathbf{A}_{n-1}\right)^{-1}\mathbf{A}_{n-1}\mathbf{U}_{n-1}\theta_m(s) - \frac{l^2}{EI}\left(\mathbf{I}_{n-1}\frac{s^2}{\omega^2} + \mathbf{A}_{n-1}\right)^{-1}\mathbf{P}_{n-1}F_t(s) \tag{19}$$

where

$$\omega^2 = \frac{n-1}{\lambda m}\frac{EI}{l^3} = \frac{(n-1)EI}{m_b l^3} \tag{20}$$

Finally, substituting Eq. (19) in Eq. (14) and reordering the resultant equation, we achieve an expression, which relates the tip angle with measured variables, coupling torque and motor angle, i.e. the first equation of the general model presented

$$\begin{aligned}\theta_t(s) = {} & \frac{\hat{\mathbf{U}}_n^{\mathrm{T}}\mathbf{A}_n}{\hat{\mathbf{U}}_n^{\mathrm{T}}\mathbf{A}_n\hat{\mathbf{U}}_n}\left[\mathbf{U}_n - \hat{\mathbf{I}}_n\left(\mathbf{I}_{n-1}\frac{s^2}{\omega^2} + \mathbf{A}_{n-1}\right)^{-1}\mathbf{A}_{n-1}\mathbf{U}_{n-1}\right]\theta_m(s) \\ & + \frac{l^2}{EI}\frac{1}{\hat{\mathbf{U}}_n^{\mathrm{T}}\mathbf{A}_n\hat{\mathbf{U}}_n}\left[\hat{\mathbf{U}}_n^{\mathrm{T}}\mathbf{A}_n\hat{\mathbf{I}}_n\left(\mathbf{I}_{n-1}\frac{s^2}{\omega^2} + \mathbf{A}_{n-1}\right)^{-1}\mathbf{P}_{n-1} + 1\right]F_t(s)\end{aligned} \tag{21}$$

On the other hand, we can rewrite Eq. (10) in the Laplace domain as

$$\Gamma_c(s) = l^2\mathbf{\Lambda}_{n-1}\mathbf{M}_{n-1}s^2\mathbf{\Theta}_{n-1}(s) - lF_t(s) \tag{22}$$

and, substituting Eqs. (12) and (19) in the previous relation, we obtain the expression for $\Gamma_c(s)$ in terms of $\theta_m(s)$ and $F_t(s)$, completing the model proposed in Eq. (1):

$$\Gamma_c(s) = \left[\frac{EI}{l}\frac{s^2}{\omega^2}\mathbf{\Lambda}_{n-1}\left(\mathbf{I}_{n-1}\frac{s^2}{\omega^2} + \mathbf{A}_{n-1}\right)^{-1}\mathbf{A}_{n-1}\mathbf{U}_{n-1}\right]\theta_m(s) - \left[\frac{s^2}{\omega^2}\mathbf{\Lambda}_{n-1}\left(\mathbf{I}_{n-1}\frac{s^2}{\omega^2} + \mathbf{A}_{n-1}\right)^{-1}\mathbf{P}_{n-1} + 1\right]lF_t(s) \tag{23}$$

Therefore, it is immediate to deduce the values of the transfer functions in $G(s)$, which are

$$\begin{aligned}G(s) &= \begin{bmatrix} g_{11}(s) & g_{12}(s) \\ g_{21}(s) & g_{22}(s)\end{bmatrix} \\ &= \begin{bmatrix} \dfrac{\hat{\mathbf{U}}_n^{\mathrm{T}}\mathbf{A}_n}{\hat{\mathbf{U}}_n^{\mathrm{T}}\mathbf{A}_n\hat{\mathbf{U}}_n}\left[\mathbf{U}_n - \hat{\mathbf{I}}_n\left(\mathbf{I}_{n-1}\dfrac{s^2}{\omega^2} + \mathbf{A}_{n-1}\right)^{-1}\mathbf{A}_{n-1}\mathbf{U}_{n-1}\right] & \dfrac{l^2}{EI}\dfrac{1}{\hat{\mathbf{U}}_n^{\mathrm{T}}\mathbf{A}_n\hat{\mathbf{U}}_n}\left[\hat{\mathbf{U}}_n^{\mathrm{T}}\mathbf{A}_n\hat{\mathbf{I}}_n\left(\mathbf{I}_{n-1}\dfrac{s^2}{\omega^2} + \mathbf{A}_{n-1}\right)^{-1}\mathbf{P}_{n-1} + 1\right] \\ \dfrac{EI}{l}\dfrac{s^2}{\omega^2}\mathbf{\Lambda}_{n-1}\left(\mathbf{I}_{n-1}\dfrac{s^2}{\omega^2} + \mathbf{A}_{n-1}\right)^{-1}\mathbf{A}_{n-1}\mathbf{U}_{n-1} & -l\left[\dfrac{s^2}{\omega^2}\mathbf{\Lambda}_{n-1}\left(\mathbf{I}_{n-1}\dfrac{s^2}{\omega^2} + \mathbf{A}_{n-1}\right)^{-1}\mathbf{P}_{n-1} + 1\right]\end{bmatrix}\end{aligned} \tag{24}$$

3. Particular cases

To illustrate the previous mathematical results, this section presents two particular cases: a beam whose mass can be neglected; and a beam with its mass concentrated at its middle point.

3.1. Beam with negligible mass

In this case, the matrix form of the dynamic model of the system presented in Eqs. (5) and (9) collapses into the two following scalar equations:

$$0 = \frac{3EI}{l^3}(\theta_m - \theta_t) + \frac{1}{l}F_t \tag{25}$$

$$\Gamma_c = -lF_t \tag{26}$$

The matrices of the system are

$$\begin{gathered}\mathbf{M}_n = 0; \mathbf{A}_n = 3; \mathbf{U}_n = 1; \hat{\mathbf{U}}_n = 1; \hat{\mathbf{I}}_n = \varnothing \\ \mathbf{M}_{n-1} = \varnothing; \mathbf{A}_{n-1} = \varnothing\, \mathbf{U}_{n-1} = \varnothing; \bar{\mathbf{U}}_n = 0; \mathbf{P}_{n-1} = \varnothing\end{gathered} \tag{27}$$

which yield the following transfer functions:

$$G(s) = \begin{bmatrix} g_{11}(s) & g_{12}(s) \\ g_{21}(s) & g_{22}(s) \end{bmatrix} = \begin{bmatrix} 1 & \dfrac{l^2}{3EI} \\ 0 & -l \end{bmatrix} \tag{28}$$

Substituting in Eq. (5), the mass estimator for a very lightweight beam yields

$$m = \frac{1}{l^2 s^2}\frac{\Gamma_c(s)}{\theta_m(s) - (l/3EI)\Gamma_c(s)} \tag{29}$$

and, applying the inverse Laplace transformation, we obtain an expression in the time domain

$$m = \frac{1}{l^2}\frac{\Gamma_c(t)}{\ddot{\theta}_m(t) - (\ddot{\Gamma}_c(t)/c)} \tag{30}$$

where $c = 3EI/l$ is the stiffness of the beam, which is supposed massless.

3.2. Beam with its mass concentrated in a single point

Now we particularize the estimator for a beam model assuming the mass to be concentrated in its middle point. For this particular case, the matrices of the model are

$$\begin{gathered}\mathbf{M}_n = \lambda m \begin{bmatrix} 1 & 0 \\ 0 & 0 \end{bmatrix}; \mathbf{A}_n = \tfrac{24}{7}\begin{bmatrix} 32 & -20 \\ -5 & 4 \end{bmatrix}; \mathbf{U}_n = \begin{bmatrix} 1 \\ 1 \end{bmatrix}; \hat{\mathbf{U}}_n = \begin{bmatrix} 0 \\ 1 \end{bmatrix}; \hat{\mathbf{I}}_n = \begin{bmatrix} 1 \\ 0 \end{bmatrix} \\ \mathbf{M}_{n-1} = \lambda m; \mathbf{A}_{n-1} = 24; \mathbf{U}_{n-1} = 1; \overline{\mathbf{U}}_n = \begin{bmatrix} 1 \\ 0 \end{bmatrix}; \mathbf{P}_{n-1} = -5\end{gathered} \tag{31}$$

Therefore, the transfer functions yield

$$G(s) = \begin{bmatrix} g_{11}(s) & g_{12}(s) \\ g_{21}(s) & g_{22}(s) \end{bmatrix} = \begin{bmatrix} \dfrac{-\frac{1}{4}s^2 + 24\omega^2}{s^2 + 24\omega^2} & \dfrac{l^2\,\frac{7}{96}s^2 + 8\omega^2}{EI\,s^2 + 24\omega^2} \\ \dfrac{2cs^2}{s^2 + 24\omega^2} & l\dfrac{-\frac{1}{4}s^2 + 24\omega^2}{s^2 + 24\omega^2} \end{bmatrix} \tag{32}$$

Then, substituting in Eq. (5), we obtain the expression of the mass estimator for this particular beam model, resulting

$$m = \frac{1}{ls^2}\frac{(2cs^2/s^2 + 24\omega^2)\theta_m(s) - \Gamma_c(s)}{-l(\frac{1}{2}s^2 + 24\omega^2/s^2 + 24\omega^2)\theta_m(s) + \dfrac{l^2}{EI}(\frac{7}{96}s^2 + 8\omega^2/s^2 + 24\omega^2)\Gamma_c(s)}$$

$$= \frac{1}{l^2}\frac{\Gamma_c(s) - \dfrac{2cs^2}{s^2+24\omega^2}\theta_m(s)}{(\frac{1}{2}s^2+24\omega^2/s^2+24\omega^2)\ddot{\theta}_m(s) - (\frac{7}{32}s^2+24\omega^2/s^2+24\omega^2)(\ddot{\Gamma}_c(s)/c)} \tag{33}$$

Comparing Eqs. (30) and (33), it is evident that the use of a more complete model increases the complexity of the estimator to a large extent, involving more demanding calculations. However, both expressions are related and it is demonstrable that Eq. (30) is a particular case of Eq. (33), by calculating the limit for this last expression when m_b tends to zero, and therefore ω tends to infinity.

3.3. Filtering the estimator

In any of the estimators derived from Eq. (5) we need the second derivative of motor angle and coupling torque, and it is well known that differentiating noisy signals, as the measurements obtained from a strain gauge, does not give a good result. Accordingly, it is not advisable to use expressions (30) and (33) in that raw form, because the gauge signal could lead us to an erroneous identification.

It is convenient to filter that signal in order to obtain correct results. Hence, we modify the general expression of estimation (5) by multiplying its numerator and denominator by the same transfer function $F(s)$, corresponding to a low-pass filter, to secure a smoother signal for the mass estimation. The pass-band filter has been discarded due to the low oscillation frequencies of our mechanical system, as the response would become very slow.

The filtered signals will be denoted with a tilde. Their transfer functions, transformed into the Laplace domain, yield

$$\tilde{N}(s) = F(s)N(s) = \left(\frac{\omega_f}{s+\omega_f}\right)^2 (g_{21}(s)\theta_m(s) - \Gamma_c(s)) \tag{34}$$

$$\tilde{D}(s) = F(s)D(s) = l^2 s^2 \left(\frac{\omega_f}{s+\omega_f}\right)^2 [(g_{11}(s)g_{22}(s) - g_{12}(s)g_{21}(s))\theta_m(s) + g_{12}(s)\Gamma_c(s)] \tag{35}$$

where ω_f represents the cut-off frequency (in rad/s) of the filter. The ω_f selection will rely on the knowledge of the physical system, that is, on the range of variation of the system natural frequencies. Specifically, it will be set to half-decade over the highest of these frequencies. The order of the filter has been inferred from numerical simulations as a trade-off between attenuation of noise and small interference on the original signals.

In the denominator of Eq. (35), the second derivative has been included into the filter solving the problems with the noisy signals. Then, we can calculate the equivalent expression in the Z-domain [15] for the parenthesis in Eq. (34) (first-order filter), and then raise to square, thereby obtaining the following discretized expression for the second-order filter:

$$\begin{aligned}\mathbf{Z}\left[\frac{\omega_f}{s+\omega_f}\right] = F_1(z) &= \sum_{\text{at poles of } G(p)} \text{Residues of } \left(\frac{\omega_f}{p+\omega_f}\frac{1}{1-e^{pT}z^{-1}}\right) \Rightarrow F(z) \\ &= F_1^2(z) = \frac{(1-e^{-\omega_f T})^2}{z^2 - 2e^{-\omega_f T}z + e^{-2\omega_f T}}\end{aligned} \tag{36}$$

where $\mathbf{Z}[\cdot]$ represents the Z-transform of an expression.

In the denominator, making use of the properties of the Z-transform, the filter yields

$$\mathbf{Z}[s^2F(s)] \cong \left(\frac{1-z^{-1}}{T}\right)^2 F(z) \Rightarrow \mathbf{Z}[s^2F(s)] \cong \frac{(1/T^2)(1-e^{-\omega_f T})^2(z^2-2z+1)}{z^2 - 2e^{-\omega_f T}z + e^{-2\omega_f T}} \tag{37}$$

This filter also limits the bandwidth of the measured signals used in the estimation of the mass. Therefore, if we adjust appropriately the cut-off frequency, ω_f, we can attenuate the measurement of the high-frequency modes so that only the first mode passes the filter, the single mass estimator becoming then valid for any model. This is a nice property, which is illustrated in the simulations section.

4. Simulation results

After describing the estimation algorithm, a set of simulations is presented for verification purposes. These simulations have been carried out with SIMULINK^{TM}, toolboxes of the numerical mathematics package MATLAB^{TM}. In Sections 4.1, 4.2 and 4.3, we assume that there is no noise in the feedback signal so no filter is provided, while in Section 4.4 a white noise term is added to it in order to simulate the noise of the measurements and estimate the shape of the control signal in the experimental tests.

4.1. Single mass model

The data used for these simulations, which are displayed in Table 1, correspond to the parameters of an actual flexible, very lightweight single-link arm existent in our laboratory. This arm consists of a slender carbon fiber beam with one end attached to the hub of a DC motor-gear set and the other to a payload, which rests over an air table. This table accomplishes two tasks: keeping the maneuver within the horizontal plane, then canceling the gravity effects; and minimizing the friction between the tip mass and the resting surface during the movement. The payload is assumed to be much bigger than the beam mass, thereby being this last negligible. Moreover we assume that it behaves as a point mass, that is, without inertia, as it is allowed to rotate freely around its vertical axis. Therefore, the beam is modeled by a simple second-order transfer function given by

$$G(s) = \frac{(3EI/ml^3)}{s^2 + (3EI/ml^3)}$$

which is used in the simulation scheme shown in Fig. 3.

On the other hand, the DC motor rotates the beam to the desired position and it is driven by means of an amplifier acting as a current controller, whose control signal, V, varies between $+3$ and -3 V. The equation ruling the motor dynamics is given by

$$\Gamma_m = KV = J_m n_r \ddot{\theta}_m + \nu n_r \dot{\theta}_m + \frac{\Gamma_c}{n_r} \tag{38}$$

where Coulomb's friction is assumed to be negligible or counterbalanced.

This dynamics can be reduced to a second order critically damped system using a control loop consisting of a PD controller and a compensation term for canceling the effect of the coupling torque. The block diagram in the Laplace domain for this motor control loop is shown in Fig. 4. A detailed derivation for this can be

Table 1
Data of the single mass platform used in simulation

l (m)	r (m)	I (m^4)	E (GPa)	c (N m)	J_m (kg m^2)	K (N m/V)	ν (N m/s)	n_r
0.7	1.40×10^{-3}	3.02×10^{-12}	123.0	1.5907	3.70×10^{-3}	0.226	56.05×10^{-3}	50:1

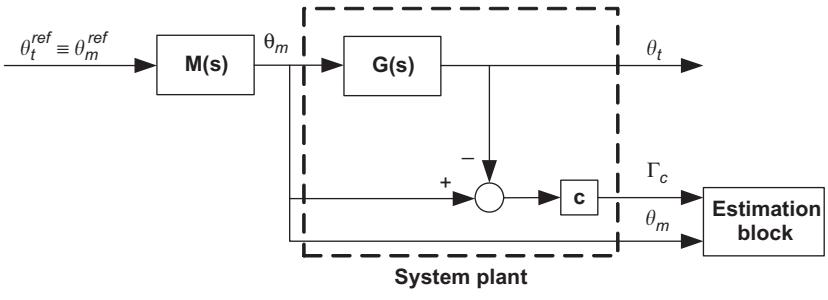

Fig. 3. Block diagram of the open-loop payload estimation.

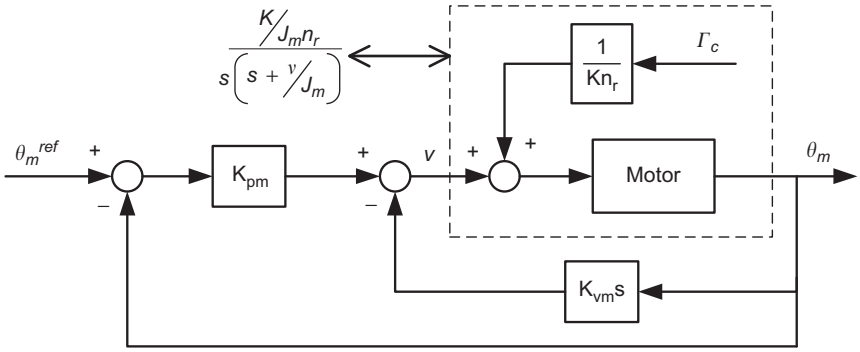

Fig. 4. Block diagram of the motor control loop.

Table 2
Identification results for the single mass model with the single mass estimator

Payload (g)	Estimated value (g)	Absolute error (g)	Relative error (%)
21.34	20.66	0.68	3.18
60.82	59.54	1.28	2.10
99.82	98.16	1.66	1.66
150.23	148.16	2.07	1.38
199.92	197.55	2.37	1.19

consulted in Ref. [16]. Then, the closed-loop motor system is modeled in simulation as

$$M(s) = \frac{\theta_m(s)}{\theta_m^{\text{ref}}(s)} = \frac{1}{(1+\alpha s)^2} \tag{39}$$

The parameters of the PD controller in the inner control loop have been calculated to obtain the critically damped dynamics for the motor given by Eq. (39), with $\alpha = 0.02$. Then, the PD constants turn out to be $K_{pm} = 40.91$ and $K_{vm} = 1.388$.

On the other hand, as the simulation model is assumed to have no noise, the filter is not necessary, so it will not be included this time in the estimation block.

We must now decide when the mass estimation can be considered stable. To determine this, and hence the final estimation of mass, we will compute continuously the mean and the standard deviation of the last j samples, until standard deviation falls below a limit, σ_m. Then, the estimated value for the tip mass will be the last calculated mean.

This process has been tested through a wide range of masses, between 20 and 200 g (the exact values are detailed in Table 2), and the simulation results are displayed in Figs. 5 and 6. The reference is a linear trajectory with constant velocity $\dot{\theta}_t = \dot{\theta}_m = 1\,\text{rad/s}$. The number of samples used in the computation of statistical parameters is 40, while the standard deviation limit for accepting the mass value has been established in $\sigma_m = 10^{-3}\,\text{kg}$. The initial conditions of the mean and the standard deviation have been set to $-2\,\text{kg}$, which is a non-possible value very different from the real range of tip masses, in order to test the convergence property in an adverse scenario.

We observe in Fig. 5 that mass estimation steadies very quickly, typically before 0.4 s, and its value is very near to the actual payload, always below the 4% error. This percentage of error is not significant and is due to the use of statistical measurements, which introduce some inaccuracies in addition to the criteria for stopping the identification. The detailed results can be checked in Table 2. In the graphs, it is also noticeable that the estimation seems not to work properly at some periodical instants. These moments correspond to the zero crossings of the tip acceleration, which can be observed in Fig. 7 (which is used in the denominator of the mass estimator in the general expression (4)), as our arm is simulated to maneuver in open-loop mode (only the

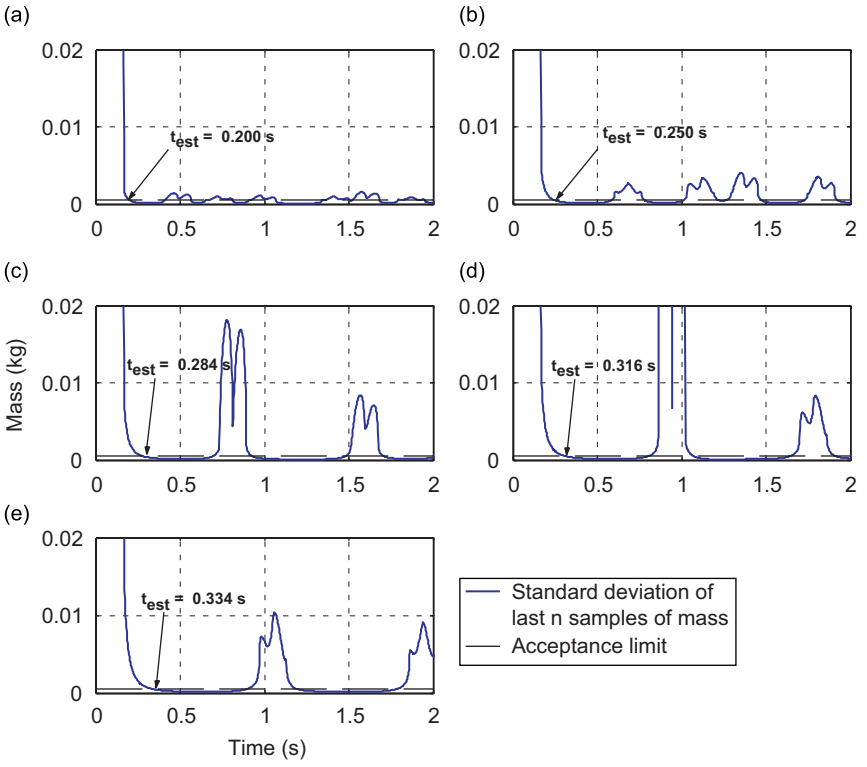

Fig. 5. Standard deviations of the identification process for a single mass model for the following masses: (a) 0.021 kg; (b) 0.061 kg; (c) 0.100 kg; (d) 0.150 kg and (e) 0.200 kg.

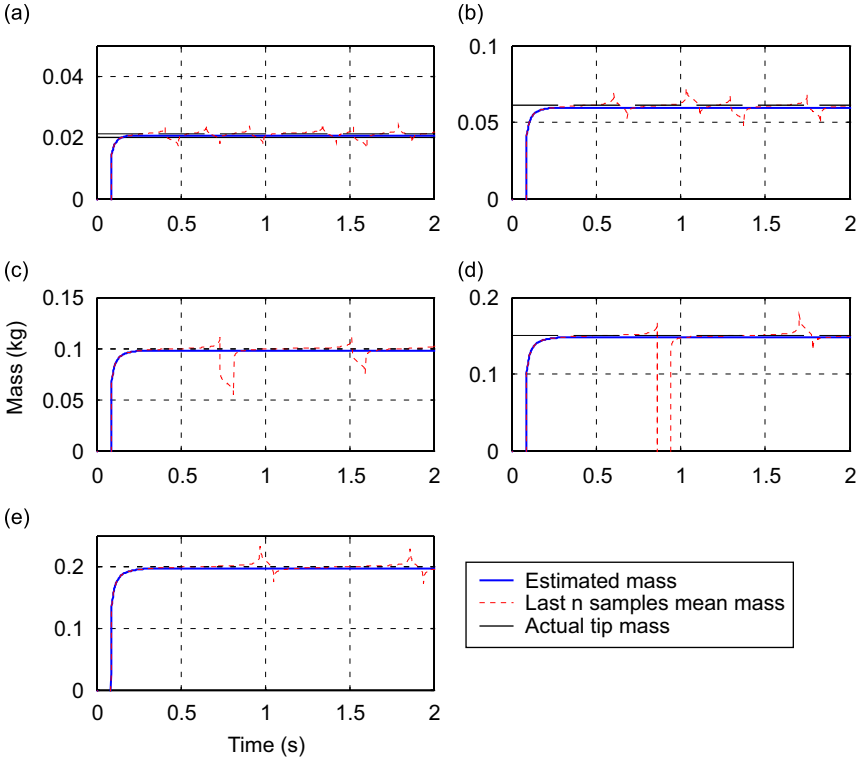

Fig. 6. Mass estimation in open loop for a single mass model. Tip masses: (a) 0.021 kg; (b) 0.061 kg; (c) 0.100 kg; (d) 0.150 kg and (e) 0.200 kg.

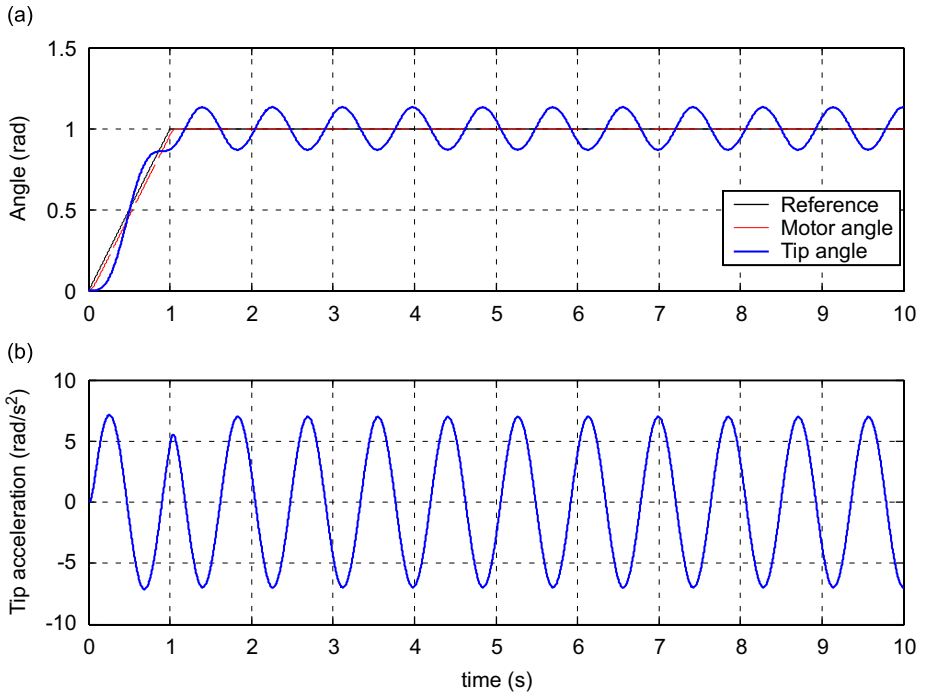

Fig. 7. Simulated arm response in open loop (a) shows motor and tip positions while (b) displays tip acceleration evolution.

motor position loop is closed). In a tip controlled motion, as it is shown afterwards with the addition of a PD adaptive controller, these zero crossings rarely take place.

4.2. Concentrated masses model

Once the correctness of the algorithm has been verified for the single mass model, a more detailed model for the flexible robot is now analyzed. Our purpose here is to study the performance of low-order estimators when dealing with higher order models. To carry out the simulation tests, the concentrated masses model developed in Ref. [14] has been adopted.

4.2.1. Single mass estimator

A two masses state-space model has been calculated for the flexible arm. The state-space equations are given by

$$\begin{bmatrix} \dot{\theta}_1 \\ \dot{\theta}_2 \\ \ddot{\theta}_1 \\ \ddot{\theta}_2 \end{bmatrix} = \begin{bmatrix} 0 & 0 & 1 & 0 \\ 0 & 0 & 0 & 1 \\ -\dfrac{1536}{7}\dfrac{EI}{\lambda M_p L^3} & \dfrac{480}{7}\dfrac{EI}{\lambda M_p L^3} & 0 & 0 \\ \dfrac{120}{7}\dfrac{EI}{M_p L^3} & -\dfrac{96}{7}\dfrac{EI}{M_p L^3} & 0 & 0 \end{bmatrix} \begin{bmatrix} \theta_1 \\ \theta_2 \\ \dot{\theta}_1 \\ \dot{\theta}_2 \end{bmatrix} + \begin{bmatrix} 0 \\ 0 \\ \dfrac{288}{7}\dfrac{EI}{\lambda M_p L^3} \\ -\dfrac{24}{7}\dfrac{EI}{M_p L^3} \end{bmatrix} \theta_m$$

$$\begin{bmatrix} \theta_1 \\ \theta_2 \\ \Gamma_c \end{bmatrix} = \begin{bmatrix} 1 & 0 & 0 & 0 \\ 0 & 1 & 0 & 0 \\ -\dfrac{72}{7L} & \dfrac{24}{7L} & 0 & 0 \end{bmatrix} \begin{bmatrix} \theta_1 \\ \theta_2 \\ \dot{\theta}_1 \\ \dot{\theta}_2 \end{bmatrix} + \begin{bmatrix} 0 \\ 0 \\ \dfrac{48}{7L} \end{bmatrix} \theta_m \tag{40}$$

Table 3
Identification results for the concentrated masses model with the single mass estimator

Payload (g)	Estimated value (g)	Absolute error (g)	Relative error (%)
21.34	23.36	2.02	9.47
60.82	62.40	1.58	2.60
99.82	101.85	2.03	2.03
150.23	151.46	1.23	0.82
199.92	200.07	0.15	0.08

Table 4
Identification results for the concentrated masses model with the two masses estimator

Payload (g)	Estimated value (g)	Absolute error (g)	Relative error (%)
21.34	26.41	5.07	23.76
60.82	66.95	6.13	10.08
99.82	104.34	4.52	4.47
150.23	154.45	4.22	2.81
199.92	205.62	5.70	2.85

Then, the results of the tip mass identification are summarized in Table 3. Obviously, as the ratio between the tip mass and the beam mass decreases, the tip estimation worsens and the relative error augments because the beam mass interferes and changes significantly the main natural frequency of the system. However, the errors are still acceptable and quite good in most of the studied cases. In these estimated values, it has been taken into account that the inertia seen from the basis of the beam is slightly greater than the actual tip inertia, due to the addition of the beam mass into the model. Therefore, a correction factor has been applied to the estimations. Specifically, the estimation of the real payload is given by $m = m_e - \frac{1}{4}m_b$, where m_e is the estimation given by Eq. (30) for the payload. Figures containing the standard deviation and the mass estimation of the identification process are not displayed, as they are very similar to those of Section 4.1.

4.2.2. Two masses estimator

The estimator found in Eq. (33) is here applied to the two masses model detailed in Eq. (40). The results, including the correction due to the beam inertia, are displayed in Table 4. They are worse than those achieved with the single mass estimator and the estimation times are higher.

4.3. Distributed masses model

The same analysis performed in previous section is now carried out for a distributed masses model for the flexible link, which is truncated for two and three natural frequencies, respectively. This model is based on the pseudo-pinned formulation presented in Ref. [17], which, by solving numerically the characteristic equation of the partial differential equation governing the flexible link, obtains a space-state model representation for the flexible arm. The evolution of the tip mass estimation is shown in the following graphs. Specifically, Figs. 8 and 9 show the tip mass identification by means of a single mass model estimator for a robot model truncated at its second vibrational mode and Table 5 presents the numerical results.

Finally, the estimator obtained from the two masses model has also been applied to the distributed masses model truncated on the second mode of vibration, with the results shown in Table 6. These results are very close to those achieved with a simpler estimator. The graphs of the identification process are omitted again as they are again very similar to those of Figs. 8 and 9.

As a consequence of the simulation results presented in this section, it is derived that both, the simple and the two masses estimators, produce a similar identification of the payload. Theoretically, the complete estimator should approximate better the solution, as it is based in the model used for simulating the link, but,

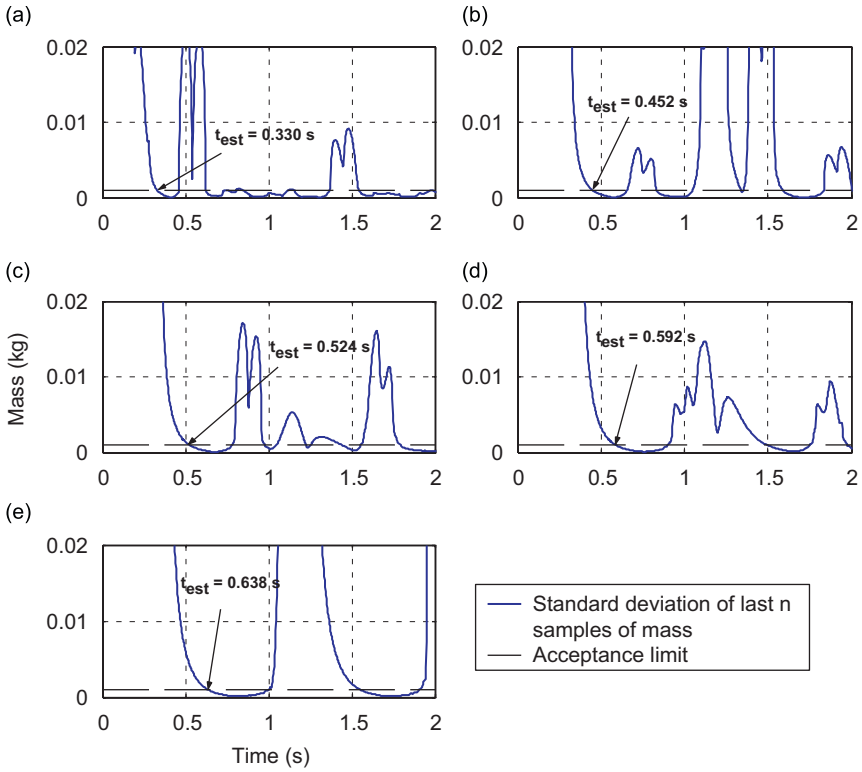

Fig. 8. Standard deviations of the identification process for a distributed masses model truncated in two vibration modes with a single mass estimator. Tip masses: (a) 0.021 kg; (b) 0.061 kg; (c) 0.100 kg; (d) 0.150 kg and (e) 0.200 kg.

in the end, the numerical errors accumulate because the estimator becomes more complicated and, hence, the final errors are similar. The obvious choice is then to use the simplest estimator, and this solution will be adopted in the application example.

4.4. Application to adaptive control

To illustrate the usefulness of this identification algorithm, an adaptive PD controller has been designed for the vibration control loop of the flexible robot, as shown in Fig. 10. The model chosen for the robot, which accurately depicts the experimental rig described in following Section 5.1, consists of a massless link driven by a DC motor actuator. It carries a single, point payload, which is attached at the end of the beam.

Firstly, we calculate the PD constants, K_p and K_v, for the nominal mass, $m = 60\,\mathrm{g}$, with the following specifications: no overshoot, $M_p = 0\%$, and small settling time, $t_s = 1\,\mathrm{s}$. The results are $K_p = -0.7963$ and $K_v = 0.07447$. The tip position is not directly measured, but estimated with the aid of the coupling torque and the motor angle measurements by means of following expression:

$$\theta_t = \theta_m - \frac{1}{c}\Gamma_{\mathrm{coup}} \tag{41}$$

obtained by combining Eqs. (25) and (26).

A noise term is added to the coupling torque to simulate the experimental measures of the strain gauges, which are very noisy. From the experimental measurement of our sensing system, the variance of this noise have been set to $10^{-5}\,\mathrm{N\,m}$. Therefore, we now need to filter the mass estimation as explained in Section 3.3. The selected cut-off frequency for the estimator filter is $\omega_f = 10\,\mathrm{rad/s}$, what, applied to Eqs. (36) and (37), and

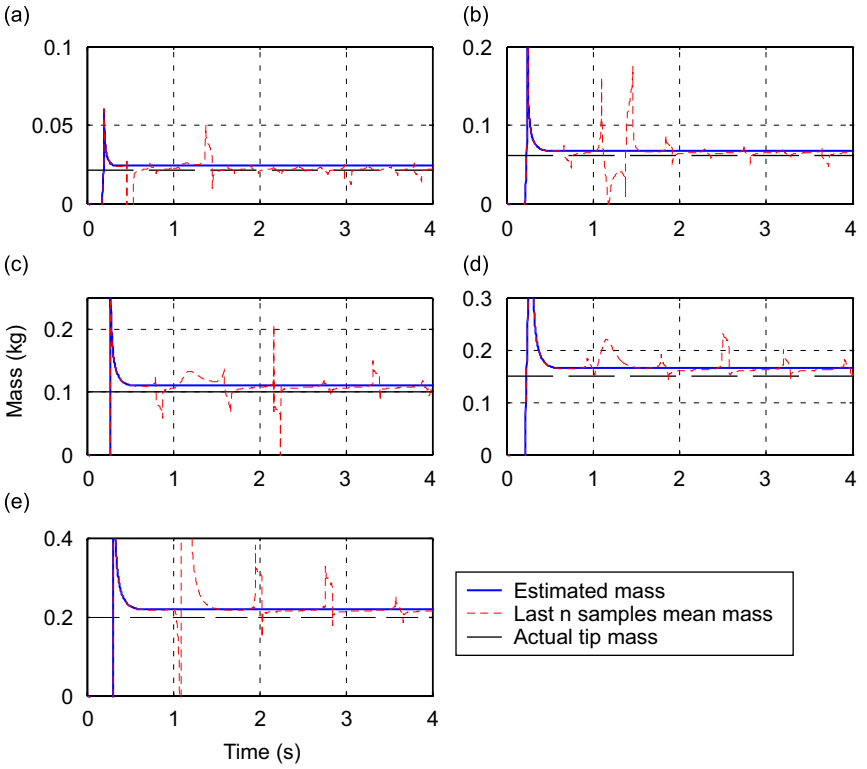

Fig. 9. Estimation for a distributed masses model truncated in two vibration modes with single mass estimator. Tip masses: (a) 0.021 kg; (b) 0.061 kg; (c) 0.100 kg; (d) 0.150 kg and (e) 0.200 kg.

Table 5
Identification results for the distributed masses model with the single mass estimator

Payload (g)	Estimated value (g)	Absolute error (g)	Relative error (%)
21.34	23.75	2.41	11.29
60.82	67.11	6.29	10.34
99.82	109.48	9.66	9.67
150.23	164.13	13.90	9.25
199.92	217.94	18.02	9.01

Table 6
Identification results for the distributed masses model with the two masses estimator

Payload (g)	Estimated value (g)	Absolute error (g)	Relative error (%)
21.34	23.14	1.80	8.43
60.82	66.27	5.45	8.96
99.82	109.98	10.16	10.18
150.23	162.47	12.24	8.15
199.92	221.16	21.24	10.62

particularized for the a sample time $T = 0.002$ s, yields

$$F(s) = \frac{10^2}{(s+10)^2} \quad \rightarrow \quad \mathbf{Z}[F(s)]_{T=0.002} \cong \frac{0.0198^2 z^2}{z^2 - 1.961z + 0.961} \tag{42}$$

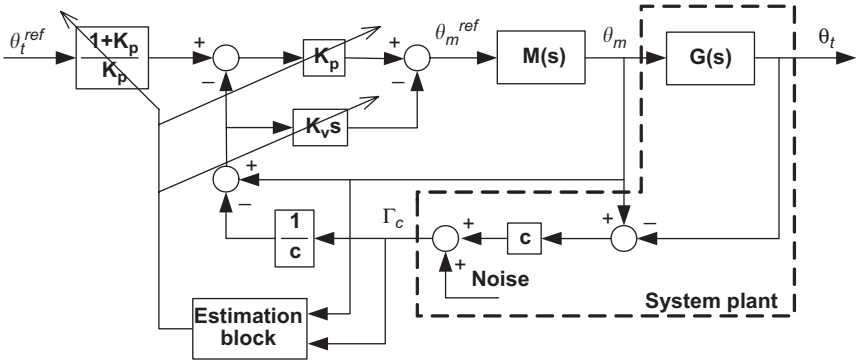

Fig. 10. Adaptive outer control loop based in payload identification.

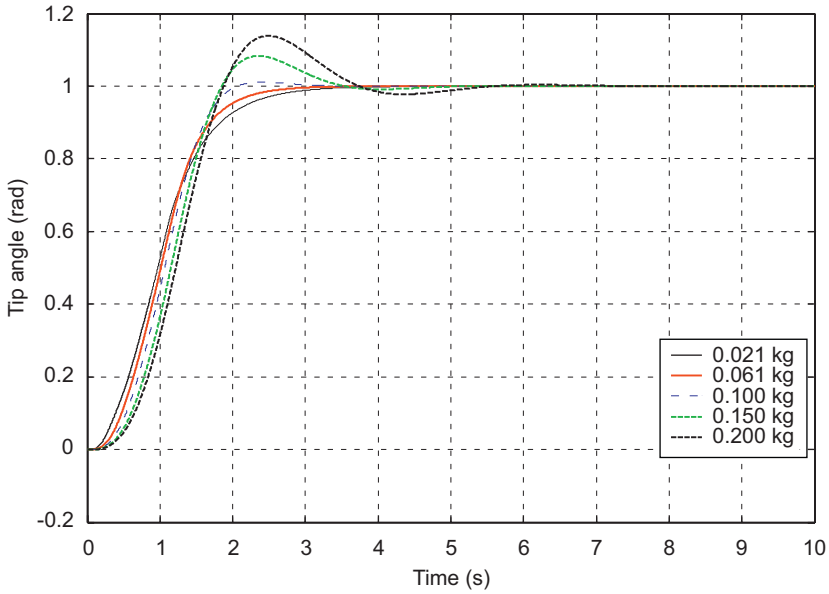

Fig. 11. Simulation of the tip mass position with a nominal PD controller for different tip masses.

$$\mathbf{Z}[s^2F(s)]_{T=0.002} \cong \frac{98.023z^2 - 196.046z + 98.023}{z^2 - 1.961z + 0.961} \tag{43}$$

Now we will perform the maneuvers for each of the masses considered for the system, that is, from three times lighter than nominal, $m_m = 20\,\text{g}$, to more than three times heavier, $m_m = 202\,\text{g}$. In Fig. 11, the tip mass position during the maneuver when using the PD controller for the nominal case is displayed. It is noticeable the high overshoot that appears for payloads bigger than nominal, reaching the 14% for the 200 g mass. On the other side, the lightest mass performs slightly slower than the nominal one. These results advise the use of a control scheme insensitive to payload variations, such as adaptive control, to fulfill the requirements imposed to the system for the whole range of masses. Fig. 12 shows the control signal applied for each simulation. Due to the noisy nature of these signals, it is very difficult to discriminate any differences between the different masses. This voltage control is actually very similar for all of them, but slightly delayed in time for the bigger masses.

Taking advantage of the identification algorithm (30), we will determine the appropriate controller for each experiment. The simulation begins with the nominal PD parameters and, whenever the estimation process finishes, these parameters are tuned according to the actual payload, as shown in Table 7. The results are

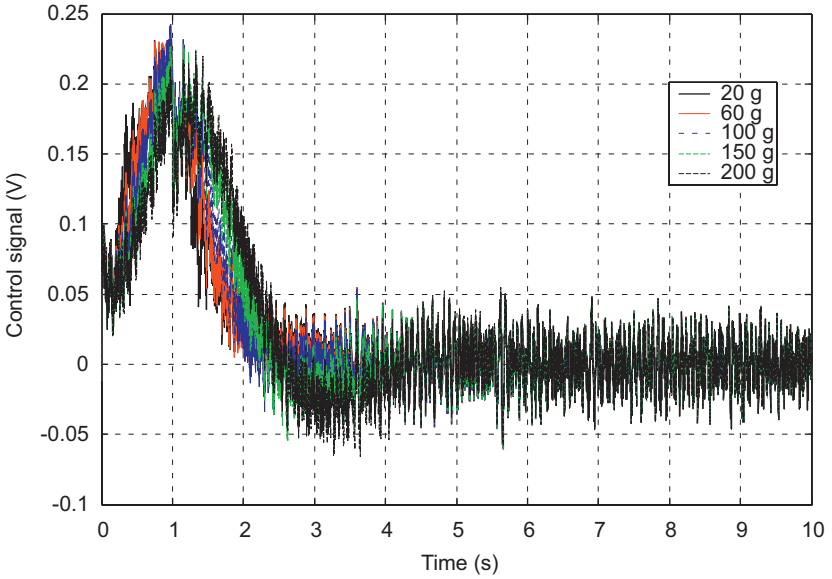

Fig. 12. Simulation of the control signal with nominal PD controller for different tip masses.

Table 7
PD Controllers for different payloads

Payload (g)	K_p	K_v
21.34	−0.9227	0.003248
60.82	−0.7963	0.07447
99.82	−0.6697	0.1458
150.23	−0.4780	0.2538
199.92	−0.3203	0.3427

displayed from Figs. 13 to 15. From comparing the system responses with and without adaptive control, the improvements are obvious. Overshoot has been completely removed while settling time has been reduced and kept nearly the same for every mass. The estimation time in closed-loop maneuvers is very similar to its counterpart in open-loop maneuvers (around 0.5 s), while the estimation error is slightly bigger as can be observed in Table 8.

Results in Table 8 have been obtained performing a series of two thousand simulations, with different seeds for the generation of the white noise signal, and calculating the average values for the estimation of the mass. No one of the simulations ended with an erroneous estimated value.

5. Experimental validation

This section presents the experiments carried out both for verifying the estimation process in open-loop maneuvers and for testing the adaptive control.

5.1. Description of the experimental setup

The experimental rig is shown in Fig. 16. The link is a 3 mm diameter, solid carbon fiber bar attached in one end to the hub of a Harmonic Drive mini servo DC motor RH-8D-6006-E036AL-SP(N) which has a reduction relation $n_r = 50$. A disk that can freely rotate around its vertical axis is placed at the other end. Due to this free

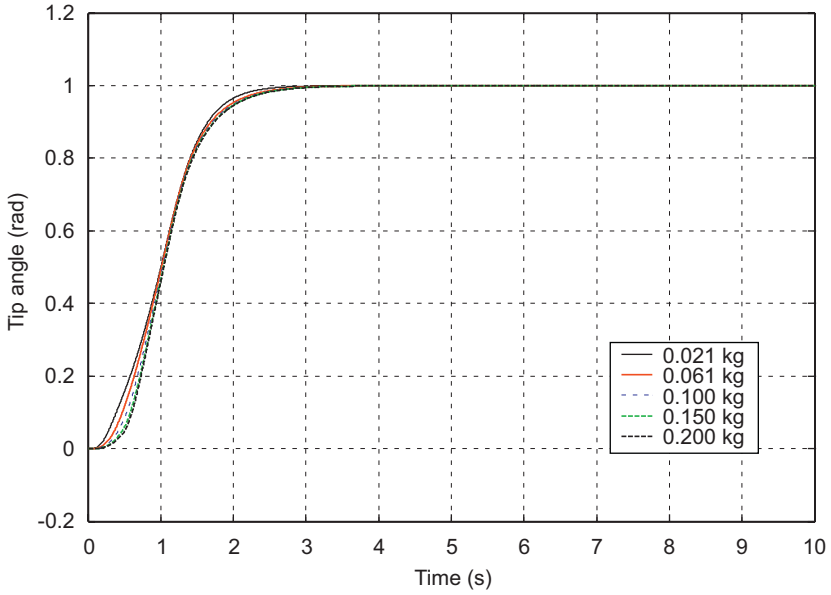

Fig. 13. Simulation of the tip mass position with adaptive PD controller for different tip masses.

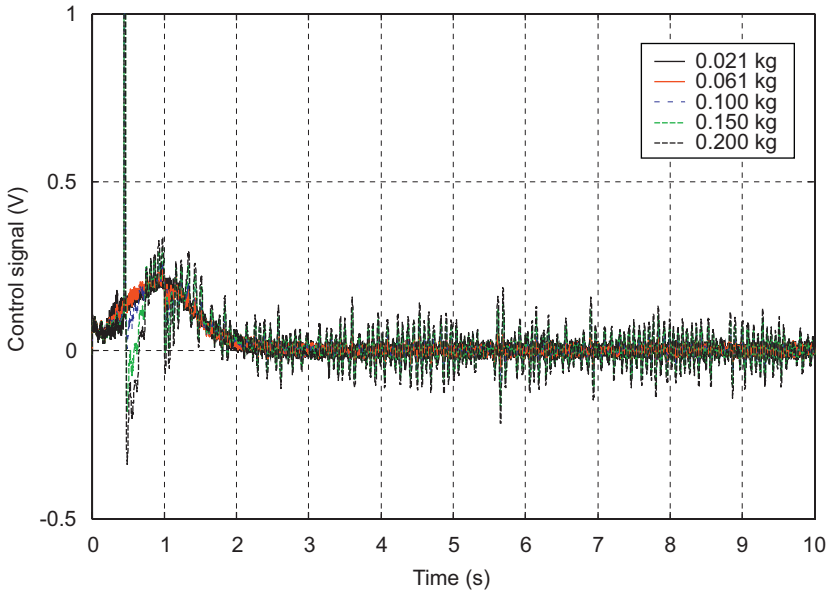

Fig. 14. Simulation of the control signal with adaptive PD controller for different tip masses.

rotation, the tip mass can be considered as a point mass, that is, its rotational inertia is equal to zero. This payload is floating over an air table in order to cancel gravity effects that would make the beam bend on the vertical direction. Then, the maneuver is performed in a horizontal plane with a minimum component of friction between the table and the disk.

On the other hand, the sensorial system consists of a couple of KYOWA KFG-5-120-C1-11 strain gauges in a half-bridge configuration. The gauge signals are adapted with the signal conditioner DPM-602A from

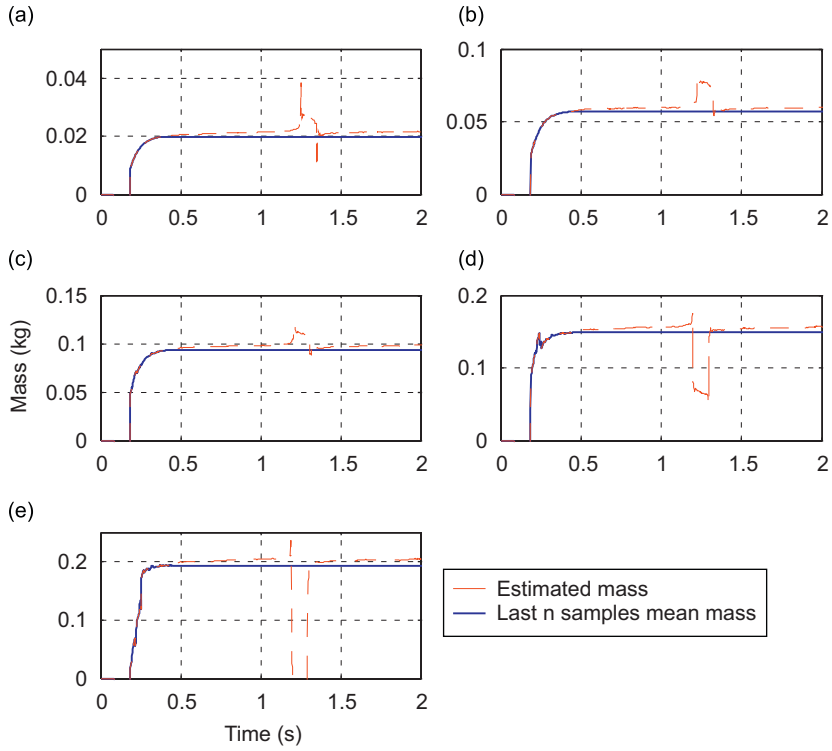

Fig. 15. Simulation of the mass identification process when the system is governed by a PD controller with different payloads. Tip masses: (a) 0.021 kg; (b) 0.061 kg; (c) 0.100 kg; (d) 0.150 kg and (e) 0.200 kg.

Table 8
Identification results for the closed-loop adaptive control application (single mass model and single mass estimator)

Payload (g)	Estimated value (g)	Absolute error (g)	Relative error (%)
21.34	19.60	1.74	8.15
60.82	56.90	3.92	6.44
99.82	93.62	6.20	6.21
150.23	148.60	1.63	1.08
199.92	192.87	7.05	3.53

KYOWA and are read from the PC with a National Instruments PCI-6024E data acquisition board. These gauges measure the strain of the beam at the base, which is directly proportional to the coupling torque. In addition, an optical incremental encoder measures the motor angle with a precision of 7×10^{-5} rad. These two measurements are used in the identification of the mass. Moreover, they are also used in the outer control loop to estimate the tip position used in the feedback for the PD controller.

5.2. Experimental results

A set of experiments emulating the simulations has been carried out in the real platform. The payload has been adapted with disks of different masses to cover the proposed range of operation, from 20 to 200 g. Firstly, the tip angle responses when using the PD nominal controller with every mass are shown in Fig. 17. The behavior is similar to the obtained in simulation, with bigger overshoots for the heavier masses. The only difference is the small oscillations that can be observed in the detail of Fig. 17, which corresponds to the

Fig. 16. Photo of the experimental setup.

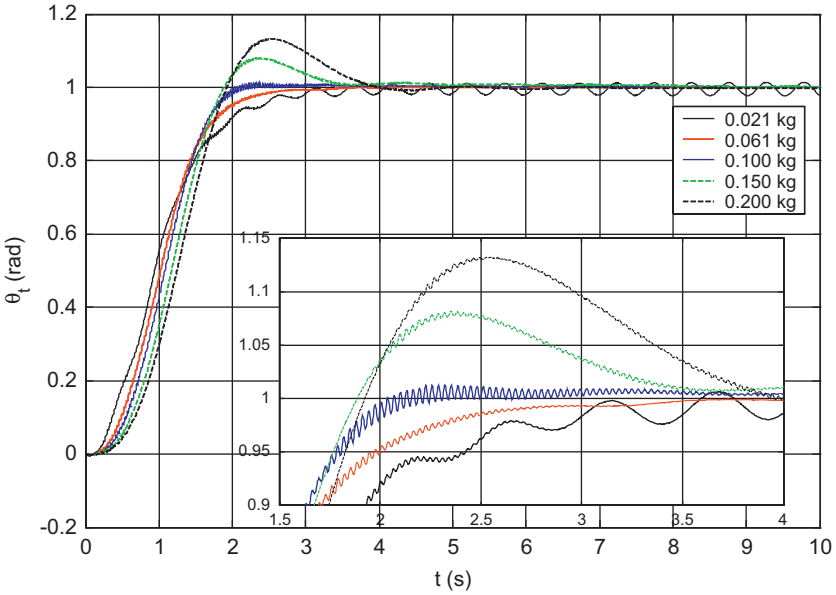

Fig. 17. Experimentally measured tip angle for different masses when the system is controlled with the nominal PD constants.

second mode of vibration of the system, which had been assumed negligible in the model, and, hence, has not been cancelled. This phenomenon, known as spillover [18], can be usually overlooked in systems with a high payload–beam mass ratio, as it is rapidly damped and its amplitude is small. However, for the lightest payload, which is only three times heavier than the beam, this effect is noticeable and causes the arm to become unstable without the appropriate controller. The control signal injected for the motor remains quite uniform, in terms of maximum values, for all the experiments.

Applying jointly the mass identification process and the selection of the appropriate PD control, we obtain the dynamical response shown in Fig. 18. The mass identification evolution is displayed in Fig. 19. Its accuracy is in the same range than in simulation, below 11% error, while the time of estimation is between the 0.41 s for the 20 g mass and the 0.89 s for the 200 g disk. The specific figures for the estimation process are presented in Table 9.

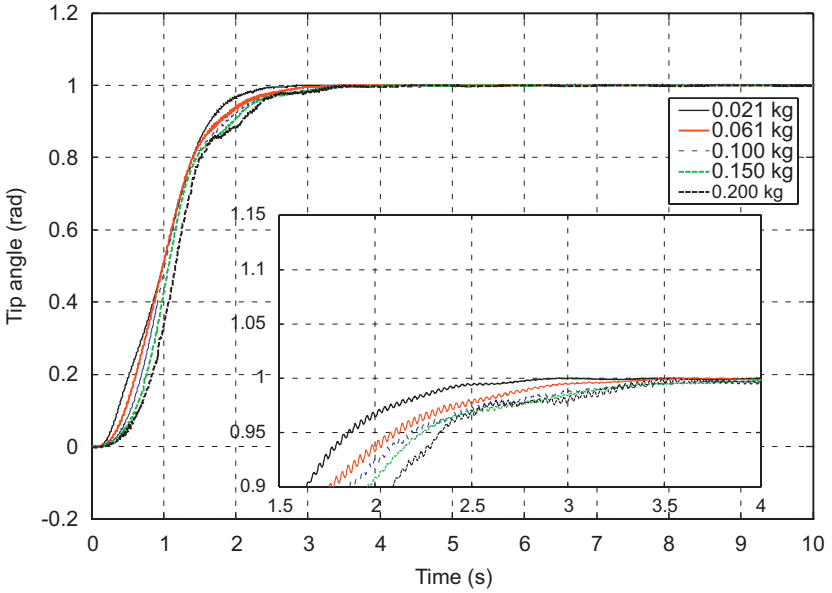

Fig. 18. Tip angle evolution during the maneuver when the beam is governed by an adaptive PD controller.

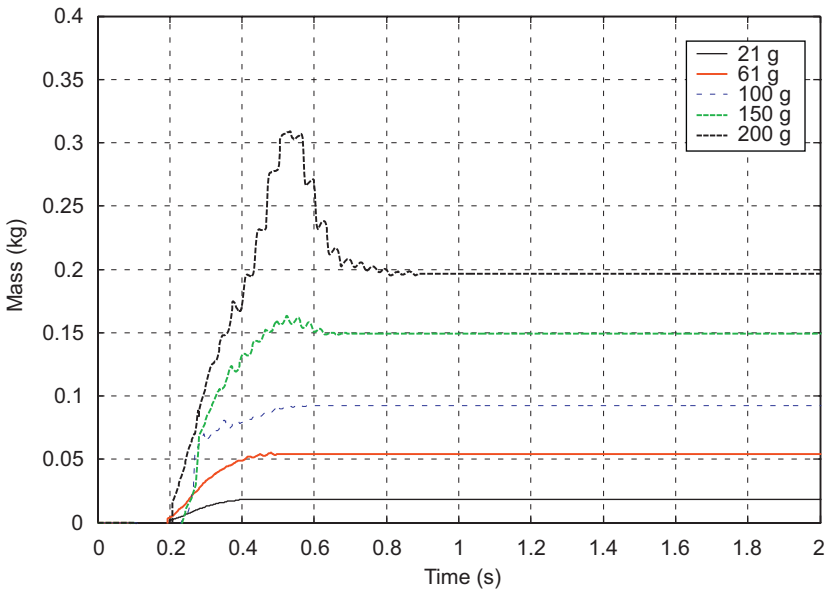

Fig. 19. Evolution of mass identification during experiments.

6. Conclusions

This work describes a new, generic estimator for the payload of a flexible robot, which is the most changeable parameter in a robot configuration (e.g. pick and place applications) and strongly influences the system dynamics. This estimator can be adapted to any of the common models used to describe flexible links: concentrated masses models or truncated distributed masses models. The estimator is independent of the actuator dynamics and only needs the measurements of the motor angle and the coupling torque at the base.

Table 9
Identification results of the experiments using a single mass estimator

Payload (g)	Estimated value (g)	Absolute error (g)	Relative error (%)
21.34	19.60	1.74	10.50
60.82	55.10	2.92	9.40
99.82	92.22	7.60	7.61
150.23	149.02	1.21	0.81
199.92	196.29	3.63	1.82

Along the paper, a set of simulations with models of different complexity has been carried out, proving the estimator to be robust enough for a wide range of systems.

The addition of a filter improves the performance of the estimation process because it attenuates the noisy nature of the strain gauges. It can also be used to diminish the effect of the higher order non-modeled vibration modes (*spillover*), and actually, allows the use of a simpler estimator even when higher modes are not negligible, as explained in the simulation section.

Finally, an application to the adaptive control of a rest-to-rest motion of a flexible robot has been implemented. This example illustrates the usefulness of the estimator, which calculates the payload online during the maneuvers. The efficiency of the PD controller is outstandingly improved with the joint use of the adaptive controller and the estimation method. The simulation results are completely supported by the experimental results obtained in an experimental platform.

Acknowledgments

The authors wish to thank the financial support provided by the Spanish Government (under CICYT contract Ref.: DPI2006-13834), the Junta de Comunidades de Castilla-La Mancha and the European Social Fund.

References

[1] S.K. Dwivedy, P. Eberhard, Dynamic analysis of flexible manipulators, a literature review, *Mechanism and Machine Theory* 41 (2006) 749–777.
[2] A. Benosman, G.L. Vey, Control of flexible manipulators: a survey, *Robotica* 22 (2004) 533–545.
[3] C. Sallaberger, Robotics and control R&D in the Canadian space station program, *Proceedings of the Canadian Conference on Electrical and Computer Engineering*, Calgary, Canada, 1996, pp. 482–485.
[4] K.J. Aström, B. Wittenmark, *Adaptive Control*, Addison-Wesley, United States of America, 1995.
[5] A. Koivo, K. Lee, Self-tuning control of planar two-link manipulator with nonrigid arms, *Proceedings of the 1989 IEEE International Conference on Robotics and Automation*, Scottdale, May 1989, pp. 1030–1035.
[6] R. Cannon, D. Rovner, Experiments toward on-line identification and control of a very flexible one link manipulator, *International Journal of Robotics Research* 6 (1987) 3–19.
[7] B. Siciliano, B.-S. Yuan, W.J. Book, Model reference adaptive control of a one link flexible arm, *Twenty-fifth IEEE Conference on Decision and Control*, *Athina*, December 1986, pp. 91–95.
[8] C.J. Damaren, Adaptive control of flexible manipulators carrying large uncertain payloads, *Journal of Robotic Systems* 13 (1996) 219–228.
[9] E.G. Christoforou, C.J. Damaren, The control of flexible-link robots manipulating large payloads: theory and experiments, *Journal of Robotic Systems* 17 (2000) 255–271.
[10] J.J. Feliu, V. Feliu, C. Cerrada, Load adaptive control of single-link flexible arms based on a new modeling technique, *IEEE Transactions on Robotics and Automation* 15 (1999) 793–804.
[11] J.R. Trapero, H. Sira-Ramírez, V.F. Batlle, A fast on-line frequency estimator of lightly damped vibrations in flexible structures, *Journal of Sound and Vibration* 307 (2007) 365–378.
[12] H. Unbehauen, G.P. Rao, A review of identification in continuous-time systems, *Annual Reviews in Control* 22 (1998) 145–171.
[13] P. Young, Parameter estimation for continuous-time models—a survey, *Automatica* 17 (1981) 23–29.
[14] V. Feliu, K.S. Rattan, H.B. Brown, Modeling and control of single-link flexible arms with lumped masses, *Journal of Dynamic Systems, Measurement and Control—Transactions of the ASME* 114 (1992) 59–69.

[15] K. Ogata, *Modern Control Engineering*, Prentice-Hall, Englewood Cliffs, NJ, 2001.
[16] V. Feliu, F. Ramos, Strain gauge based control of single-link flexible very lightweight robots robust to payload changes, *Mechatronics* 15 (2005) 547–571.
[17] F. Bellezza, L. Lanari, G. Ulivi, Exact modeling of the flexible slewing link, *Proceedings of the 1990 IEEE International Conference on Robotics and Automation*, Cincinnati, May 1990, pp. 734–739.
[18] M.J. Balas, Feedback-control of flexible systems, *IEEE Transactions on Automatic Control* 23 (1978) 673–679.